Nano Trends 10 (2025) 100116

Contents lists available at ScienceDirect

Nano Trends

journal homepage: www.elsevier.com/locate/nantre

A resistive electron irradiation microsensor made from conductive electrospun polycaprolactone fibers loaded with carbon nanotubes and fullerene C60

Fabricio N. Molinari [a,b], Maria A. Mancuso [b], Emanuel Bilbao [c], Gustavo Giménez [c], Leandro N. Monsalve [a,d,e,*]

[a] INTI Textiles, Av. Gral. Paz 5445, San Martín, Buenos Aires, Argentina
[b] Institute of Atmospheric Pollution Research—National Research Council (IIA—CNR), Research Area of Rome 1, Strada Provinciale 35d, 9-00010 Montelibretti, Italy
[c] INTI Micro y Nanotecnologías, Av. Gral. Paz 5445, San Martín, Buenos Aires, Argentina
[d] Instituto de la Calidad Industrial (INCALIN – INTI – UNSAM), Av. Gral. Paz 5445, San Martín, Buenos Aires, Argentina
[e] Consejo Nacional de Investigaciones Científicas y Técnicas (CONICET), Godoy Cruz 2290 CABA, Argentina

ARTICLE INFO

Keywords:
Conductive nanocomposite
Resistive sensor
Dosimeter

ABSTRACT

In this work electron radiation microdevices were fabricated and characterized. The microdevices consisted of aligned conductive electrospun fibers made of polycaprolactone loaded with multiwalled carbon nanotubes and C60 deposited onto gold interdigitated microelectrodes. They were capable of permanently increasing their conductivity upon exposure to electron beam irradiation from 0.02 pC μm^{-2} accelerated at 10 and 20 keV. This phenomenon could be explained due to the ability of C60 to trap and stabilize negative charges and thus contribute to the conductivity of the polymer composite. The microdevices achieved their maximum conductivity after an irradiation between 0.22 and 0.27 pC μm^{-2} and this maximum was dependent of the electron acceleration. Montecarlo simulations were performed to explain dependence as function of electron penetration in the polymer composite. Moreover, the microdevices irradiated at 20 keV maintained their final conductivity and the microdevices irradiated at 10 keV increased their final conductivity after 6 days from irradiation. C60 proved to act as highly efficient electron scavengers within the polymer composite and contribute to its conductivity, and the microdevices have potential application as beta radiation sensors.

1. Introduction

Electron beams are generated through acceleration and collimation of electrons from an electron source using strong electric fields in vacuum. They have multiple applications: electron microscopy, welding, sterilization and radiotherapy among others. For the case of radiotherapy, calibration of the beam in terms of the dose administrated to a patient is critical in order to ensure the safety and efficacy of the treatment. Normally, different types of dosimeters are employed for the calibration of electron beams: polymer gels [1–4] or radiochromic films [5] for less accurate measurements and alanine films or pellets for more accurate measurements [6,7]. However, the response of these dosimeters has to be measured using spectrophotometry or electron paramagnetic resonance, which makes continuous monitoring of radiation during radiotherapy difficult. Scintillators made of radioluminescent polymer nanocomposites are also used for real-time monitoring of ionizing radiation [8,9].

On the other hand, electronic microdosimeters whose primary signal is electrical are much more suitable for continuous monitoring and ensuring homogeneous irradiation. For instance, commercial MOSFET dosimeters were successfully employed for monitoring electron beam irradiation for intraoperative radiation therapy [10,11]. MOSFETs can serve as dosimeters since charges generated and trapped within the gate insulator by radiation shifts permanently their threshold volage (V_T). However, the application of MOSFETs for electron radiation therapy dosimetry is limited by their cost and reproducibility. Another way for real-time monitoring of electron beams is the use of devices made of polymers or polymer composites that change their electrical properties upon irradiation [12]. In this case, a polycarbonate layer loaded with bismuth oxide nanoparticles was used for the fabrication of a sensor that

* Corresponding author at: INTI Textiles, *Av.* Gral. Paz 5445, San Martín, Buenos Aires, Argentina.
E-mail address: monsalve@inti.gob.ar (L.N. Monsalve).

https://doi.org/10.1016/j.nwnano.2025.100116
Received 21 December 2024; Received in revised form 3 May 2025; Accepted 4 May 2025
Available online 5 May 2025

detects beta radiation by producing an electric current during irradiation. Graphene and graphene nanocomposites also change their electrical properties when irradiated with beta radiation. For instance, reduced graphene oxide was used for the fabrication of a field effect transistor that increases its channel resistance and decreases its capacitance upon irradiation [13]. Another example is the use of a PVA/-graphene composite as an active layer between *n*-type silicon and gold in a Schottky diode [14]. In this case, the irradiation increases the interface states between *n*-type silicon and the PVA/graphene layer thus lowering the series resistance of the diode.

C60/polymer composites are well-known electron scavengers due to the electronic properties of C60 [15]. C60 has a strong electron affinity (estimated at 2.66 eV, the same energy of a photon falling in the blue region of the visible spectrum) and acts as a *n*-type semiconductor when used as channel in field effect transistors [16]. Moreover, charge injection in C60/polymer composites can cause ionization of C60, which enhances the electrical conductivity of the composite. This feature has been employed for the fabrication of C60-based memory devices [17–21]. The mechanism for achieving the electrical conductivity of a C60-syndiotactic polymethyl methacrylate nanocomposite was studied by Qi et al. by quantum mechanics calculations, and it was found that short molecular wires of negatively charged C60 that trap an average of 2.7 to 3.5 electrons per molecule.

Electrically conductive fibers are currently widely used for many commercial applications (i.e.: ESD garments). However, current research is focusing on the application of different conductive materials on fibers (carbon nanomaterials, semiconductor polymers, MXenes) for the fabrication of stimuli-responsive textile materials [22]. Such materials can be used as active layers in sensors, such as physical and chemical sensors. Specially, electrospinning is a very attractive technique for the fabrication of nonwoven conductive stimuli-responsive nonwoven textile materials [23]. Electrospinning is a simple and scalable process that can be used for the obtention of fibers of submicrometer diameter made of organic, inorganic and hybrid composite materials with different morphologies and component distribution (porous, core-shell, hollow), which confers high surface area and controlled distribution of the different phases of the textile material.

Based on our previous work involving the fabrication of memory devices based on electrospun polycaprolactone with carbon nanotubes and C60 [20], we decided to test their ability to sense electron radiation and investigate their potential application as low-cost and reproducible dosimeters.

2. Materials and methods

2.1. Materials

PCL (Mw 80,000, Sigma-Aldrich, catalog number 1002,600,432), C60 (99.9 %, Sigma-Aldrich, catalog number 379,646), polyvinyl pyrrolidone PVP K30 (Anedra, Argentina), multiwalled carbon nanotubes (MWCNT) (Nanocyl 7000, Belgium), xylene, toluene, hexane, DMF, and acetone (Sintorgan, Argentina) were reagent grade and used straight from the bottle.

2.2. Preparation of polymer solutions

C60 (35 mg) was dissolved in xylene (11 ml) in ultrasound bath (240 W, 40 kHz) at 40 °C for 90 min. Then 2.7 g of PCL was added to 10 ml of the C60-xylene solution and dissolved at 50 °C under magnetic stirring. The resulting solution was mixed with 10 g of a dispersion of MWCNTs in DMF (0.7 % wt.) prepared according to a previously described procedure [24]. Once homogeneous, an additional 1 g of PCL was dissolved under magnetic stirring for 3 h and used immediately.

2.3. Electrospinning conditions and microdevice fabrication

A Y-flow electrospinner 2.2.D-500 (Y-flow SD, Spain) was used for electrospinning. Distance to the collector was optimized in order to obtain regular and dry fibers. The fibers were collected at 25 °C and a relative humidity range between 60 and 70 %. Different tests determined 26 cm as the optimum distance between the needle and the collector. The flow rate of the solution was 1 $ml.h^{-1}$ and the diameter of the needle was 450 μm for all samples. A rotary drum collector was employed to produce mats of aligned fibers. The setup included two high voltage sources: one at the needle between +6 and +12 kV and the other at the collector between −15 and −17 kV. A rotation speed of 500 rpm was selected for the collector in order to obtain aligned fibers.

PCL-MWCNT/C60 solutions were electrospun onto interdigitated sputtered gold electrodes of different width to length (W/L) ratio (L = 10–50 μm, W = 500–10.000) patterned on a Si/SiO_2 (300 nm) substrate for 15 min using a rotary collector to align the fibers perpendicular to electrode fingers (Fig. 1). The dies with the deposited fibers were annealed at 60 °C for 20 min to improve contact between fibers and electrodes.

2.4. Morphological characterization

Scanning electron microscopy and Focused Ion Beam (FIB) experiments were performed in a Helios Nanolab 650 (FEI). Fiber diameter, alignment and surface coverage measurements were carried out by analysis of SEM images using Image J software [25].

2.5. Electron irradiation

Electron irradiation was performed in a Helios Nanolab 650 (FEI). Doses (D) were calculated according to recommendations published by Egerton [26]. Microdevices of different areas (0.018 – 0.625 mm^2) were selected individually and irradiated with a fixed current of 0.8 nA (I_b) for three minutes (t), and scan frequency of 300 ns (f) and a Dwell time of 35 ns (Dw) for three minutes in a given irradiation area (A) so that they all received a charge of 15.8416 nC. The dose was given as a function of the area of each of the microdevices according to Eq. (1):

$$D = \frac{I_b \cdot t \cdot Dw}{A \cdot f} \quad (1)$$

In these experiments it is difficult to define an exact dose, so the dose was time controlled with the previously cited parameters. A very soft imaging condition were used (1 kV and 50 pA) in order to minimize the irradiation in the visualization of each microdevice, so that the penetration is minimal. and proceeded as quickly as possible to choose the irradiation area, since it is necessary to irradiate the sample in order to visualise the microdevices, focus and select the area of irradiation.

2.6. Electrical characterization

Electrical characterization was performed using a Keithley 4200 SCS equipped with a manual probe station (Wentworth Lab AVT 702). Two voltage sweeps from −0.2 to 0.2 V were applied between electrodes (voltage and current were measured every 0.01 V at a scan rate of 0.1 V s^{-1}). Mean resistance was calculated from the slope of current vs. voltage plot in the linear region nearest to zero voltage. Each electrode was tested before and after the exposure to electron beam radiation in order to evaluate changes in the electrical resistance of the material. The irradiated electrodes were tested once a day for 6 days to test the effect of the radiation on the material's electric properties in time. Four different microdevices have been tested in each experiment.

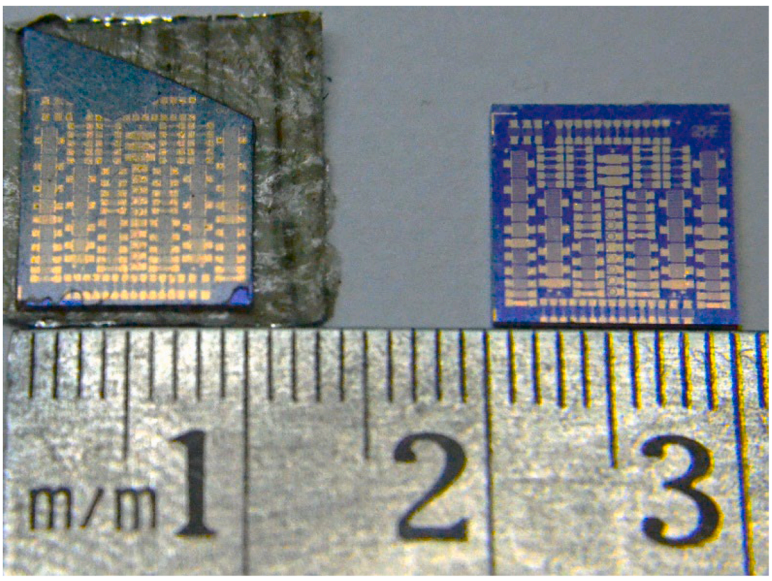

Fig. 1. 1 cm x 1 cm Si/SiO_2 die with interdigitated microelectrodes and electrospun fibers (left) and without electrospun fibers (right).

3. Results and discussion

3.1. Fiber characterization

SEM images of microdevices were taken to characterize fiber morphology (Fig. 2). These images revealed a monolayer of fibers aligned perpendicular to electrode fingers. Regular fibers with smooth surfaces were observed. It was observed that the thermal treatment performed for the optimization of the electrical properties of the microdevices did not affect the fibrous structure of the electrospun layer.

Diameter and angle respect to the electrode fingers distribution were analyzed and the results are summarized in Table 1. Surface coverage was analyzed using color threshold tool of the image J software [25]. This tool allowed us to determine the area that fibers are occupying in the image compared to the total area of the image. The calculation of areas and porosity are shown in Table 2. It could be observed that fibers were deposited as a submicron-thick and porous layer and that are mostly perpendicular to the electrode fingers.

Regarding their nanostructure, the fibers contain a dispersion of MWCNTs decorated with C60. The fibers were characterized by SEM, STEM, XRD, DSC and Raman spectroscopy. XRD diffractogram of PCL-MWCNT/C60 fibers (Figure S2) shows a downshift of the 2θ peak that corresponds to (111) lattice plane of PCL crystal phase, which indicates a reduction of the crystal thickness with the presence of C60 [27]. DSC thermograms (Figure S3) shows that PCL-MWCNT/C60 fibers have lower crystallization temperature compared to PCL-MWCNT fibers. This is due to the association of C60 with MWCNTs, hindering the latter to act as nucleating agents for PCL during crystallization. Raman spectra of PCL-MWCNT/C60 fibers (Figure S4) confirms this assumption by showing a downshift in the pentagonal pinch mode of C60 from 1469 cm^{-1} to 1458 cm^{-1}. This downshift is an indicator of the association between C60 and carbon nanotubes [28]. These C60/MWCNT complexes are responsible of their electrical switching properties and it has been demonstrated previously that charge injection at a given electrical potential through gold contacts promoted a decrease of their electrical

Table 1
Average diameter and angle of electrospun PCL-MWCNT/C60 fibers.

Fiber diameter (nm)	650 ± 18
Angle respect to the electrode fingers (°)	91.3 ± 0.4

Table 2
Analysis of surface coverage.

Total area of image	67,374 μ^2
Fibers' area	13,226 μ^2
Surface coverage $\left[\frac{Fibers\ Area}{Total\ Area} x100\right]$	20 %

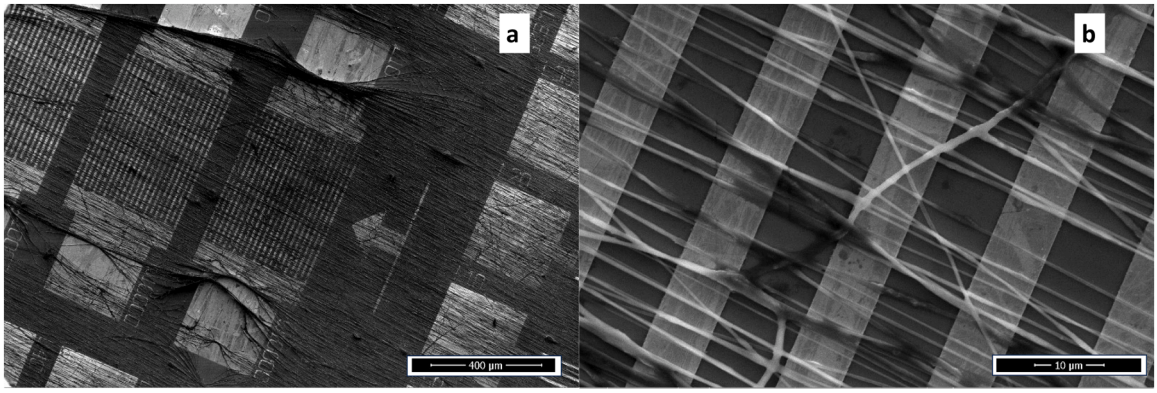

Fig. 2. SEM images of PCL-MWCNT/C60 electrospun fibers deposited onto interdigitated electrodes at 100x (a) and 2500x (b).

resistance [20]. This phenomenon happens due to the presence of C60 at the surface of MWCNTs that trap some of the electrons and enhances the electrical contact between MWCNT/C60 complexes. Similarly, electrons originated from an electron irradiation source with enough energy to penetrate the fibers and be trapped by C60 can cause the same effect.

3.2. Electrical properties

As stated in our previous work, these PCL-MWCNT/C60 fibers reveal a resistive switching effect associated with an accumulation of negative charges by C60/MWCNT complexes. The devices were stimulated by passing a current through them generating a decrease in devices' resistance which was dependent on the bias voltage [20]. Surface resistivity of pristine fibers was 4.94×10^8 Ω/sq. When used as a memory device and a programming voltage was applied through the electrodes their resistance decreased down to 25 % of its original value.

The decrease of electrical resistance can be explained by the generation of new conduction paths made of short wires of negatively charged C60 between neighboring MWCNTs (Fig. 3). According to the characterization of the composite, C60 molecules are surrounding MWCNTs and therefore the contacts within the MWCNT network are mediated by C60.

In this work, the possibility of stimulating the microdevices by irradiation with an electron beam was explored. For this purpose, an experiment was designed using a scanning electron microscope as a source of electrons and the microdevices as targets. During the experiment, microdevices fabricated using interdigitated electrodes with incremental active areas were irradiated using accelerated electrons at 10 kV and 20 kV. A nonlinear behavior in the I vs. V slope when the microdevices are subjected to a voltage sweep from −1 to 1 V or more could be verified (Figure S5). On the other hand, it was found that a voltage sweep of a shorter range (−0.2 to 0.2 V) showed a linear and constant behavior that was used in further experiments to measure the electrical resistance of the microdevices without affecting them. Electrical resistance was measured for each microdevice before and after irradiation. In each case the electrical resistance was calculated using the Ohm's Law in the linear region of the current vs. voltage curve (−0.2 to 0.2 V). The slope of the curve is the electrical resistance, an increasement on the slope means a more conductive material. Fig. 4 shows the current voltage curves of microdevices before (R_0) and after irradiation (R). It is noticeable that slope of R was higher than R_0 revealing a higher conductivity after irradiation. The variation of electrical resistance was correlated with the dose and the energy of the electrons during the irradiation as shown in Fig. 4a.

Regarding concentration of C60 in the fibers, the maximum achievable concentration using the solvent systems described in the experimental section (xylene-DMF) was 0.8 %wt. in dry fibers. Although much lower than that reported in previous C60-polymer composites with electrical properties [21], it is enough for conferring electrical properties in combination with MWCNTs. However, as the electrical percolation network within the composite is a combination of C60 and MWCNTs, the concentration of MWCNTs and the C60/MWCNT ratio play a fundamental role in the electrical switching behavior of the composite. In a previous work we had determined the percolation threshold of a MWCNT network alone in electrospun MWCNT composites at 1.8 %wt [24]. Therefore, this MWCNT concentration was selected as a starting point for experiments in order to maximize the difference in electrical resistance between before and after irradiation. Accordingly, both composites prepared with 1.5 and 2.2 %wt. MWCNT and 0.8 %wt. C60 did not show significant differences in electrical resistance upon electron irradiation.

Fig. 4b shows the variation of the resistance of the microdevices for different doses applied with accelerated electrons at 10 kV and 20 kV. It could be noticed that all the microdevices present an R/R_0 value less than one regardless of the dose applied, which means that, in all cases, there was a decrease in electrical resistance after irradiation. Furthermore, it was observed that irradiation at 20 kV generates a greater resistance variation than 10 kV accelerated electrons. This phenomenon demonstrates that, since the number of electrons impacted per unit area is the same, the acceleration mainly affects the penetration of the electrons into the matrix. Regarding the reproducibility, a variability of up to 4.8 % around average values of R/R_0. This phenomenon could be explained by device variability due to different fiber coverage onto electrodes.

Fig. 5 shows the Monte Carlo simulations using the open-source software Casino V2.5[29] that were carried out in order to obtain the hypothetical penetration of electrons in the fibers. Fiber density was estimated from the chemical formula of the repeating unit of PCL ($C_6H_{10}O_2$). The physical model was the Rutherford model and the number of trajectories simulated were 100,000 with a microscope beam radius of 15 nm. In the simulation, it was noticed that the electrons can penetrate the whole layer with 50 % of their initial energy at 20 kV of acceleration (a monolayer of fibers has an average diameter of 650 nm), while they penetrate 260 nm at 50 % of the initial energy at 10 kV. Electrons can trespass the whole layer only with an average 10 % of their initial energy.

By penetrating further and with greater energy, electrons with sufficient energy can be trapped by the C60/MWCNT complexes that are found within the fibers not only at the surface but in the whole fiber's volume. Electrons scavenged by C60 molecules allow the formation of new conduction channels and produce a further decrease in electrical resistance. Another highlighted point was that both curves had a similar shape, reaching a minimum resistance for a dose of 0.27 pC μm^{-2} and then showing an increase in resistance for higher doses. This increase in resistance could be associated with over-stimulation of the microdevice. This effect was also observed in devices powered with voltage cycles reported previously [20]. Probably, the super accumulation of charges blocks/breaks some conduction channels, thus generating an increase in resistance.

In order to evaluate the stability over time of the decrease in electrical resistance induced by an electron beam, the resistance value on the microdevices was measured after 2 and 6 days from irradiation. Fig. 6

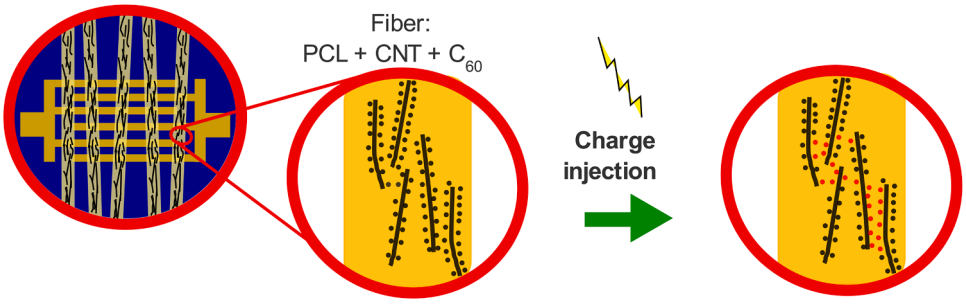

Fig. 3. Graphical representation of MWCNT/C60 complexes within PCL fibers and their response to charge injection. Short molecular wires of negatively charged C60 (red) are formed between neighboring MWCNTs increasing their electrical contacts.

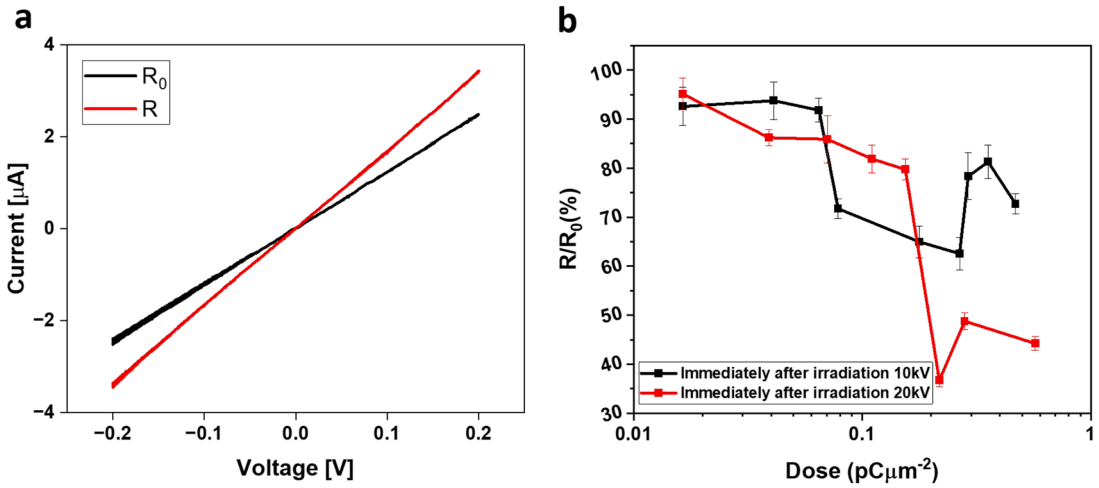

Fig. 4. Current-Voltage curve of a microdevice before(R_0) and after irradiation (R) (a). Relative resistance referred to the resistance of microdevices before irradiation as function of dose of electrons accelerated at 10 kV (black squares) and 20 kV (red squares) (b).

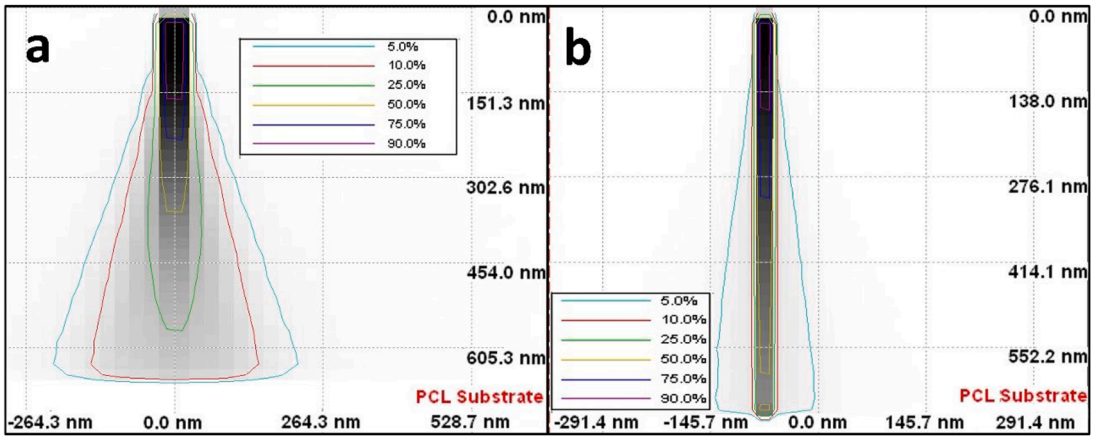

Fig. 5. Simulated electron beam penetration in PCL fibers at 10 kV (a) and 20 kV (b).

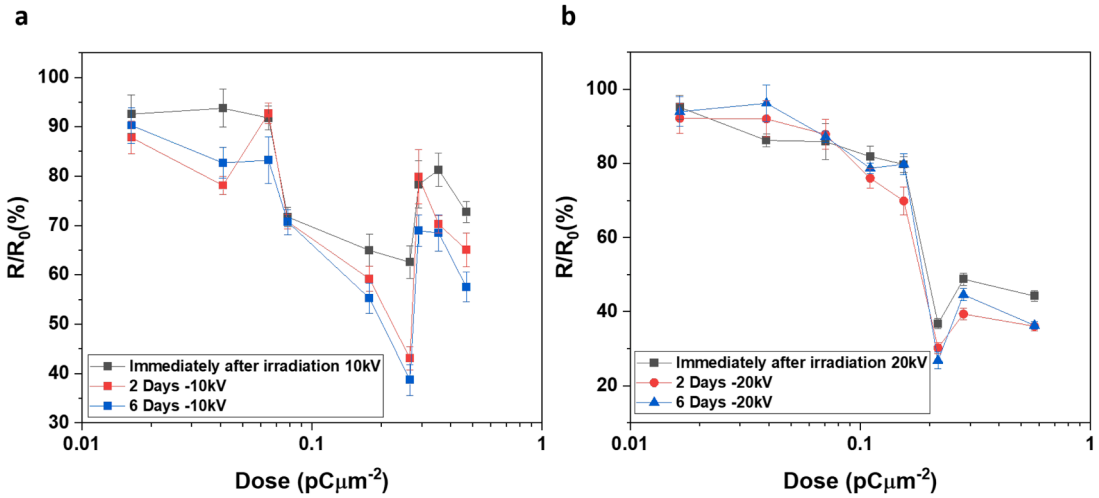

Fig. 6. Relative resistance referred to the resistance of microdevices before irradiation (R_0) as function of dose and time after irradiation of electrons accelerated at 10 kV (a) and 20 kV (b).

shows the evolution of the relative resistance of the microdevices as a function of electron dose and time after irradiation.

Microdevices irradiated at 10 kV lowered their resistance over time after irradiation event. This decrease in electrical resistance was more pronounced at a dose of 0.27 pC μm^{-2} after 6 days from irradiation, which was 70 % of its original value immediately after irradiation and

reached 40 % after 6 days. Interestingly, this effect was much less pronounced when the microdevices were irradiated at 20 kV. This phenomenon could be related to electron beam penetration. Charge accumulation in the fibers takes place during irradiation and it's proportional to the dose. However, to impact in the electric resistance these charges have to be scavenged by C60 molecules. When irradiated at 10 kV, the electrons do not have sufficient energy to trespass the fiber width. Some of them are trapped by C60 leading to a decrease in electrical resistance and the remaining electrons produces ionization in the PCL molecules with no immediate impact in the electrical properties. However, these ionized PCL molecules are able to migrate within the polymer matrix and transfer their charge to C60 molecules not previously affected by the electron beam leading to a secondary reduction of electrical resistance within days after electron irradiation. On the other hand, microdevices irradiated at 20 kV did not show such large change in electrical resistance over time after irradiation as electron beam is able to penetrate the whole volume of the fibers and ionize C60 molecules more effectively. This hypothesis is supported by dielectric relaxation experiments carried out by Grimau et al. on PCL. Authors showed that, at 30 °C, quasistatic charges have sufficient mobility within the polymer to migrate and rearrange [30].

Another feature of the microdevices is that their electrical resistance reaches a minimum at a dose of 0.27 pC μm^{-2} and 0.22 pC μm^{-2} at 10 and 20 kV respectively. The minima for R/R_0 were 41 % and 30 % at 10 and 20 kV respectively, which is consistent with our previous results regarding resistive switching behavior of the same PCL-C60/MWCNT electrospun fibers. These minima can be regarded as saturation points at which every C60 molecule was fully ionized. The ratio between the electrons and C60 molecules can be estimated as follows: The quantity of irradiated electrons (n_e) in a given area A is calculated by dividing the dose (D_0) by the charge of a mole of electrons (Q) (Eq. (2)):

$$\frac{n_e}{A} = \frac{D_0}{Q} \tag{2}$$

This gives between 2.28 and 2.80 $\times$ 10^{-18} mol μm^{-2} of electrons for achieving minimum electrical resistance.

On the other hand, the molecular density of C60 (n_{C60}/A) in the electrospun fibers can be calculated from the mass fraction of C60 ($C = 0.8$ %), the density of the composite (δ=1.145 $\times$ 10^{-12} g μm^{-3}, estimated from the density of PCL), the thickness of the fibers' layer ($E = 0.65$ µm, estimated from the average thickness of a single fiber), the surface coverage of the fibers' layer ($P = 20$ %) and the molecular weight of C60 (Mr_{C60}=7.21 $\times$ 10^2 g mol^{-1}) (Eq. (3)):

$$\frac{n_{C60}}{A} = E * \delta * \frac{C \cdot P}{10.000 \cdot Mr_{C60}} \tag{3}$$

Which gives 1.65 $\times$ 10^{-18} mol μm^{-2} of C60.

According to simulations conducted by Qi et al. on C60 molecular wires, the number of electrons per C60 needed for achieving a decrease of electrical resistance was 3.5 in 4-molecule-long wires and 2.7 for 10-molecule-long wires [21]. In our case, the ratio of electrons to C60 at the maxima decrease of electrical resistance was between 1.38 and 1.7. This fact demonstrates that there is a quantitative reaction between the electrons and C60 being the scavenging yield of C60 very high. These microdevices are very efficient reacting with incident electrons and have potential application for monitoring beta radiation during radiotherapy, similar to commercial MOSFET sensors [10,11].

In the case of these microdevices made of electrospun polymer composite fibers, they have the potential advantage of exposing many microdevices to a single beam and having a sensing layer of similar density and composition to biological tissue, thus allowing precise and in vivo monitoring of radiation dose and uniformity.

4. Conclusions

Fibers of PCL with C60-MWCNT electrospun nanocomposite were used for the fabrication of beta radiation microdevices based on the change of its electrical properties upon electron scavenging of C60. The microdevices were irradiated using an electron scanning microscope. They were sensitive to electron irradiation, showing a minimum of electrical resistance proportional to electron acceleration at 10 kV and 20 kV. For electrons irradiated at 10 kV the electrical resistance decreased over time after irradiation and this effect was due to incomplete penetration of the electron beam across the fibers and charge reconfiguration due to the mobility of polymer chains. Both microdevices have shown a minimum R/R_0 for doses between 0.22 and 0.27 pC μm^{-2}. The ratio of incident electrons to C60 molecules at minima of electrical resistance was calculated between 1.38 and 1.7. This demonstrates that PCL/C60-MWCNT electrospun fiber are very efficient as electron scavengers and are potentially useful as an active material for the fabrication of microdevices sensitive to beta radiation for application to monitoring radiation dose and homogeneity on radiotherapy.

CRediT authorship contribution statement

Fabricio N. Molinari: Writing – original draft, Visualization, Validation, Methodology, Investigation, Data curation, Conceptualization. **Maria A. Mancuso:** Writing – review & editing, Investigation. **Emanuel Bilbao:** Writing – review & editing, Methodology, Investigation. **Gustavo Giménez:** Writing – original draft, Validation, Methodology, Formal analysis. **Leandro N. Monsalve:** Writing – original draft, Supervision, Resources, Project administration, Methodology, Funding acquisition, Conceptualization.

Declaration of competing interest

The authors declare that they have no known competing financial interests or personal relationships that could have appeared to influence the work reported in this paper.

Acknowledgements

The authors are grateful to INTI for financial support. LM is CONICET research staff member.

Supplementary materials

Supplementary material associated with this article can be found, in the online version, at doi:10.1016/j.nwnano.2025.100116.

References

[1] G. Massillon-Jl, R. Minniti, M.G. Mitch, M.J. Maryanski, C.G. Soares, Phys. Med. Biol. 54 (2009) 1661–1672.
[2] G. Massillon-JL, R. Minniti, C.G. Soares, M.J. Maryanski, S. Robertson, Appl. Radiat. Isot. 68 (2010) 144–154.
[3] C.-S. Wuu, P. Schiff, M.J. Maryanski, T. Liu, S. Borzillary, J. Weinberger, Med. Phys. 30 (2003) 132–137.
[4] K.V. Pilařová, P. Kozubíková, J. Šolc, V. Spěváček, Radiat. Phys. Chem. 104 (2014) 283–286.
[5] M. Sądel, P. Bilski, M. Kłosowski, M. Sankowska, Radiat. Meas. 133 (2020).
[6] R.B. Miller, Electronic Irradiation of Foods. An Introduction to the Technology, Springer US, Boston, MA, 2005.
[7] P. Hjortenberg, J.W. Hansen, M. Wille, Int. J. Radiat. Appl. Instrumentation. Part 40 (1989) 997–1001.
[8] K. Yamamoto, R. Shindo, S. Ohno, S. Konta, R. Isobe, Y. Inaba, M. Suzuki, Y. Hosoi, K. Chida, Sensors 24 (2024).
[9] L. Mentasti, N. Martínez, I.A. Zucchi, J. Marcazzó, G. Orellana, M. Santiago, G. Barreto, Opt. Mater. (Amst.) (2024) 150.
[10] R. Consorti, A. Petrucci, F. Fortunato, A. Soriani, S. Marzi, G. Iaccarino, V. Landoni, M. Benassi, Int. J. Radiat. Oncol. Biol. Phys. 63 (2005) 952–960.
[11] M.S. Martínez-García, F. Simancas, A.J. Palma, A.M. Lallena, J. Banqueri, M. A. Carvajal, Sensors Actuators A Phys. 210 (2014) 175–181.
[12] S.M. Safdari, S. Malekie, S. Kashian, M. Akbari, Sci. Rep. 12 (2022) 1–10.

[13] I.B. Olenych, Y.Y. Horbenko, L.S. Monastyrskii, O.I. Aksimentyeva, O. S. Dzendzelyuk, J. Nano- Electron. Phys. 16 (2024) 2–5.
[14] Ö. Abay, M. Ulusoy, E. Uyar, U. Gökmen, S.Bilge Ocak, ACS Omega 9 (2024) 23193–23201.
[15] G. Chen, R.G. Cooks, E. Corpuz, L.T. Scott, J. Am. Soc. Mass Spectrom. 7 (1996) 619–627.
[16] H. Li, B.C.K. Tee, J.J. Cha, Y. Cui, J.W. Chung, S.Y. Lee, Z. Bao, J. Am. Chem. Soc. 134 (2012) 2760–2765.
[17] P. Predeep, D. Devasia, J. Aneesh, N.M. Faseena, Microelectron. Eng. 107 (2013) 54–57.
[18] M. Jayan, R. Davis, M.P. Karthik, K. Devika, G.V. Kumar, B. Sriraj, P. Predeep, AIP conf. Proc, 020051 (2017) 1–5.
[19] A. Nakajima, D. Fujii, Appl. Phys. Lett. 106 (2015) 103302.
[20] F.N. Molinari, E. Barragán, E. Bilbao, L. Patrone, G. Giménez, A.V. Medrano, A. Tolley, L.N. Monsalve, Polymer. (Guildf) 194 (2020) 122380.
[21] S. Qi, H. Iida, L. Liu, S. Irle, W. Hu, E. Yashima, Angew. Chemie Int. Ed. 52 (2013) 1049–1053.
[22] Y. He, S. Guo, X. Zuo, M. Tian, X. Zhang, L. Qu, J. Miao, ACS Appl. Mater. Interfaces 16 (2024) 59358–59369.
[23] X. Chen, J. Wang, J. Zhang, H. Lin, M. Tian, M. Li, Y. Tian, Chem. Eng. J. 486 (2024) 150204.
[24] F. Molinari, A.V. Medrano, A. Bacigalupe, M.M. Escobar, L.N. Monsalve, Fullerenes, Nanotub. Carbon Nanostructures 26 (2018) 667–674.
[25] C. a Schneider, W.S. Rasband, K.W. Eliceiri, Nat. Methods 9 (2012) 671–675.
[26] R.F. Egerton, Ultramicroscopy. 229 (2021) 113363.
[27] B. Alp, S. Cesur, J. Appl. Polym. Sci. 130 (2013) 1259–1275.
[28] M. Barrejón, H.B. Gobeze, M.J. Gómez-Escalonilla, J.L.G. Fierro, M. Zhang, M. Yudasaka, S. Iijima, F. D'Souza, F. Langa, Nanoscale 8 (2016) 14716–14724.
[29] D. Drouin, A.R. Couture, D. Joly, X. Tastet, V. Aimez, R. Gauvin, Scanning 29 (2007) 92–101.
[30] M. Grimau, E. Laredo, M.C. Pérez Y, A. Bello, J. Chem. Phys. 114 (2001) 6417–6425.